Original Article

Antibacterial efficacy and osteogenic potential of mineral trioxide aggregate-based retrograde filling material incorporated with silver nanoparticle and calcium fluoride

Min-Yong Lee [a], Hi-Won Yoon [b], Kwang-Mahn Kim [a], Jae-Sung Kwon [a,c*]

[a] *Department and Research Institute of Dental Biomaterials and Bioengineering, Yonsei University College of Dentistry, Seoul, South Korea*
[b] *Department of Conservative Dentistry, Gangnam Severance Hospital, Yonsei University College of Dentistry, Seoul, South Korea*
[c] *BK21 FOUR Project, Yonsei University College of Dentistry, Seoul, South Korea*

Abstract *Background/purpose:* The retrograde filling material, particularly mineral trioxide aggregate (MTA) employed in apicoectomy, should possess high antibacterial efficacy and osteogenic potential. We evaluated the antibacterial efficacy, biocompatibility, and osteogenic potential following the addition of silver nanoparticles (AgNPs) and calcium fluoride (CaF_2) in retrograde filling material of MTA.
Materials and methods: MTA was mixed with four different solvents. Group 1 (G1): distilled water, Group 2 (G2): 50 ppm AgNPs, Group 3 (G3): 1 wt% CaF_2, and Group 4 (G4): 50 ppm AgNPs and 1 wt% CaF_2. The pH variation of each group was monitored, while the surface roughness was measured. The antibacterial efficacy against *Enterococcus faecalis (E. faecalis)* and the viability of murine pre-osteoblast (MC3T3) were evaluated for each group using colorimetric assays. The gene expression levels of osteogenic potential marker (OCN, ALPL, and RUNX2) in MC3T3 cells for each group were quantified using real-time-qPCR. Statistical analysis was performed at $\alpha = 0.05$ level of significance.

* Corresponding author. Department and Research Institute of Dental Biomaterial and Bioengineering, Yonsei University College of Dentistry, 50-1 Yonsei-ro, Seodamun-gu, Seoul, 03722, Republic of Korea.
E-mail address: JKWON@yuhs.ac (J.-S. Kwon).

Results: When comparing the levels of antibacterial efficacy, the order of effectiveness was G4>G2>G3>G1 ($P < 0.05$). In the cell viability test, owing to MTA-eluted growth medium having a positive effect on MC3T3 cell proliferation, G1–4 exhibited a statistically increased cell viability compared to the control ($P < 0.05$). However, G2–4 did not result in a statistically significant difference when compared to G1 ($P < 0.05$). Moreover, G4 exhibited the highest gene expression among the four groups ($P < 0.05$).

Conclusion: The addition of AgNPs and CaF$_2$ to MTA could be a promising option for use as a new retrograde filling material.

Introduction

Incomplete filling and inadequate adjunctive treatment are the main reasons for endodontic failure following root canal treatment (RCT).[1] If the situation persists, residual microorganisms may proliferate, leading to the formation of periradicular lesions and recurrence of clinical symptoms.[2,3] Among microorganisms, *Enterococcus faecalis* (*E. faecalis*) is the primary pathogenic bacterium responsible for such lesions and clinical symptoms, as well as other problems such as chronic periodontitis.[4] If the pathological tissue of a previously treated tooth cannot be managed with repeated RCT, apicoectomy may be considered as an alternative treatment option.[5] The primary purpose of apicoectomy is the removal of bacteria from the end of the root and recovery of a resorbed apical lesion. Mineral trioxide aggregate (MTA) has been suggested as the gold standard for filling the root end cavity.[6–8] Recently, various studies have been conducted to increase the antibacterial efficacy of MTA against *E. faecalis* and its efficiency in bone regeneration.[9,10] These studies were developed by adding new materials to MTA. Silver nanoparticles (AgNPs) are excellent antibacterial agents that can combat both gram-positive and gram-negative bacteria, including *E. faecalis*. Owing to their high surface-area-to-volume ratio, AgNPs exhibit distinct physical and chemical characteristics. A previous study suggested that AgNPs penetrate the membrane of bacteria and induce bacterial permeability and consequent bacterial death.[11,12] Additionally, it has been reported that fluoride released from calcium fluoride (CaF$_2$) can modify bacterial metabolisminhibit growth[13,14] and have osteogenic potential.[15] Fluoride is known to inhibit glycolytic enzymes, including enolase. When fluoride inhibits enolase, it disrupts this glycolytic pathway, leading to a decrease in ATP production. While the antibacterial efficacy and osteogenic potential of MTA, AgNPs, and CaF$_2$ have been demonstrated individually, it has not been investigated whether the combined use of these three substances can maintain the cell viability of MTA while increasing antibacterial efficacy and osteogenic potential.

The purpose of this study was to evaluate the antibacterial efficacy against *E. faecalis*, biocompatibility of MC3T3 cells, and osteogenic potential of MC3T3 cells after the addition of AgNPs and/or CaF$_2$ to MTA.

Materials and methods

Synthesis of silver nanoparticles solution

0.3 g of chitosan (Sigma-Aldrich, St. Louis, MO, USA) was added to a solution of acetic acid (30 mL, 0.018 M, Acetic acid glacial 99%, Duksan, Ansan, Gyeonggi-do, Korea) and sonicated for 10 min, followed by 1 h of vigorous stirring at 20 °C. Thereafter, a solution of AgNO$_3$ (Sigma-Aldrich) was added to the chitosan solution and stirred for an additional hour at room temperature. The mixture was vacuum filtered through 6 μm pore filter papers (GE Healthcare, Chicago, IL, USA). NaBH$_4$ solution (Sigma-Aldrich) was added dropwise to the filtered solution under cold bath and vigorous stirring conditions for 1 h. The 1.5 mL AgNPs solution was diluted with dH$_2$O to a final volume of 10 mL. The concentration of AgNPs was measured to be 50 ppm using an inductively coupled plasma optical emission spectrometer (Agilent, Santa Clara, CA, USA).

Evaluation of photo-physicochemical property of synthesized silver nanoparticles

The synthesized AgNP solutions at concentrations of 10, 20, 40, and 80 ppm were evaluated using a UV/VIS spectrophotometer (V-650, JASCO, Oklahoma city, OK, USA) to determine the absorbance difference at various wavelengths. The morphology and particle size were evaluated by transmission electron microscopy (TEM; JEM-F200, JEOL, Akishima, Tokyo, Japan). TEM images were taken at a magnification of 100,000 × , and 186 AgNP particles were included in the TEM images. Thereafter, the length of the particles was measured using ImageJ software (NIH, Bethesda, MA, USA). Energy-dispersive X-ray spectroscopy (EDX; JEOL) was used for elemental analysis.

Fabrication of specimens

Four experimental groups were created (Table 1). The resulting mixture was transferred to a metal mold with a diameter of 10 mm and a thickness of 1 mm and allowed to set for 5 min under 95% relative humidity condition.

Table 1 The composition of four experimental groups.

	Amount of MTA	Solvent
Group 1 (G1)	150 mg	100 μL dH$_2$O
Group 2 (G2)	150 mg	100 μL dH$_2$O/50 ppm AgNPs
Group 3 (G3)	150 mg	100 μL dH$_2$O/1.5 mg CaF$_2$
Group 4 (G4)	150 mg	100 μL dH$_2$O/50 ppm AgNPs + 1.5 mg CaF$_2$

dH$_2$O; distilled water, AgNPs; silver nanoparticles, CaF$_2$; calcium fluoride.

Evaluation of surface roughness and pH variance of fabricated specimens

Two specimens were prepared for each of the four groups. The surface roughness (R$_a$) of the specimens was evaluated using an atomic force microscope (AFM; NX-7, Park Systems, Suwon, Gyeonggi-do, Korea) in noncontact mode. Each measured area was located at least 1 mm away from the other areas. To evaluate the pH variance, each specimen was prepared as described in Section 2.3. After 5 min, the specimens were immersed in 10 mL dH$_2$O and stored at 37 °C. The pH variance of the solution was evaluated for 24 h using a pH meter (Orion 4 Star, Thermo Fisher Scientific, Waltham, MA, USA). Each measurement was repeated thrice.

Bacteria culture

The study employed *E. faecalis* (ATCC 29212, Manassas, VA, USA) bacteria. *E. faecalis* was cultured in brain heart infusion broth (BHI; BD Biosciences, Franklin Lakes, NJ, USA). BHI broth was prepared by dissolving 37 g of BHI in 1 L of dH$_2$O.

Bacteria viability by colorimetric assay and live/dead baclight kit

First, the mixture of Groups 1−4 was spread on the side walls of a 96-well microplate (SPL Life Science Co., Pocheon, Gyeonggi-do, Korea) using a sharp-ended instrument. While each group was in a freshly mixed state, an optical density (OD) of 0.1 at 600 nm (OD$_{600}$), and 40 μL of *E. faecalis* suspension were carefully inoculated onto each group. The control comprised 40 μL of *E. faecalis* suspension without MTA. This 96-well microplate was incubated for 12 h at 37 °C under anaerobic conditions. Subsequently, 300 μL of phosphate-buffered saline (PBS) (Gibco, Grand Island, NY, USA) was added to each well and gently pipetted for 1 min. 50 μL of PBS-diluted bacterial suspension was divided into a new 96-well plate, to which 50 μL of fresh PBS was added. Next, 10 μL of 0.5 mg/mL MTT (3-(4,5-demethylthiazol-2-yl)-2,5-diphenyltetrazolium bromide, Sigma-Aldrich) solution was added to PBS-diluted bacterial suspension and incubated for 4 h. Finally, the 96-well plate was gently shaken for 10 min and analyzed for absorbance at 570 nm using a microplate spectrophotometer (Epoch; BioTek, Winooski, VT, USA). This procedure was repeated

thrice. Additionally, bacterial viability was determined using a live/dead baclight bacterial viability kit (Thermo Fisher Scientific) and a confocal laser scanning microscope (LSM-900; Zeiss, Oberkochen, Baden-Wurttemberg, Germany).

Cell culture

MC3T3-E1 cells are a commonly used mouse osteoblast cell line. To culture these cells, α-minimum essential medium (Gibco) growth medium was used and supplemented with 10% fetal bovine serum (FBS) (Gibco) and 1% antibiotic-antimycotic (Gibco). The cells were maintained at 37 °C in a humidified atmosphere with 5% CO$_2$.

Cell viability test by colorimetric assay and live/dead viability kit

The fabricated specimens of Groups 1−4 were allowed to set for 5 min at 37 °C. Subsequently, each specimen was placed in 2 mL of growth medium. After 24 h, the eluates were filtered using a 0.2 μm filter (Advantec, Taipei city, Taipei, Taiwan). Once the MC3T3 cells, suspended in growth medium, reached 80% confluency, 1×10^4 of them were seeded in 96 wells and incubated. After the initial seeding, cell cytotoxicity was evaluated using a water-soluble tetrazolium (WST) assay (EZ-CYTOX; DoGenBio Co., Seoul, Korea). The 100 μL elution was added to G1−4 columns. One day later, the entire liquid medium was removed and washed twice. Next, 10% Ez-CYTOX containing 100 μL growth medium was added to all of the columns, and a blank column comprised only WST solution. The wells were incubated for 3 h and the absorbance at 450 nm was analyzed using a microplate spectrophotometer (BioTek). This procedure was repeated thrice.

Additionally, the live/dead viability of MC3T3 cells after 1 d of incubation was assessed using a live/dead viability kit (Thermo Fisher Scientific) and a fluorescence microscope (EVOS FL; Thermo Fisher Scientific), and the images were captured.

Osteogenic related gene expression

Gene expression was assessed using real-time PCR. MC3T3 cells were seeded onto a six-well microplate at a density of 1×10^5 cells per well in the medium and incubated until reaching 80% confluency. After treating with growth medium and four different eluates, following the same procedure as Section 2.9, the cells were further incubated at 37 °C under a 5% CO$_2$ atmosphere for 24 h. Total RNA was isolated from each group using Trizol reagent (Invitrogen Life Tech, Carlsbad, CA, USA) and reverse-transcribed into cDNA using Accupower cyclescipt RT premix & master mix (Bioneer, Daejun, Korea). Real-time PCR analysis was performed using SYBR premix Ex Taq II (Takarka Bio, Kusatsu, Shiga-ken, Japan) on a real-time PCR system (StepOne Plus 3, Applied Biosystem, Foster city, CA, USA). The primers used in this study were osteocalcin (OCN), alkaline phosphatase (ALPL), and runt-related transcription factor 2 (RUNX2), while glyceraldehyde 3 phosphate dehydrogenase

(GAPDH) was used as the housekeeping gene. The primer sequences are listed in Table 2.

Statistical analysis

Statistical analysis was performed at $\alpha = 0.05$ level of significance and error bars in the figures represented 95% confidence interval. SPSS Statistics 23 (IBM, Armonk, NY, USA) was used for statistical analysis. The Shapiro—Wilk test was used to determine equal variances for all statistical data. One-way analysis of variance (ANOVA) was applied to these values with post-hoc analyses using Tukey's HSD.

Results

Evaluation of photo-physicochemical property of synthesized silver nanoparticles

The AgNP solution had a peak at approximately 400 nm, which remained consistent across all concentrations tested. The intensity of the absorbance peaks increased proportionally with the concentration of the AgNP solution (Fig. 1(A)). In the TEM image, they had a uniform and dispersed spherical morphology (Fig. 1(B)). The average size of the AgNPs was approximately 16 nm, and the particle size distribution closely followed a normal distribution (Fig. 1(C)). EDX analysis confirmed the presence of Ag ions (yellow color), corresponding to the morphology of the AgNPs observed in the TEM images (Fig. 1(D)).

Surface roughness and pH variance

3D images of the fabricated specimens from each group are presented, and no significant differences are observed among the images (Fig. 2(A)). No statistically significant difference was found in the R_a values of specimens among the groups (Fig. 2(B)). The pH changes of specimens with the same surface area immersed in the same amount of dH_2O for 1 d are shown (Fig. 2(C)). Groups 2 and 4 exhibited lower pH values than Groups 1 and 3 for up to 4 h. In contrast, Group 3 did not exhibit a difference from Group 1. After 5 h, there was no difference in the pH of Groups 1—4, and after 24 h, the pH converged to approximately 12 in all groups.

Bacteria viability test

In this study, bacterial viability (%) was determined using Equation (1The calculated bacterial viability (%) was thereafter compared between the different groups.

$$\text{Bacterial viability (\%)} = (\text{Exp.} - \text{Blank}) / (\text{Control} - \text{Blank}) \times 100 \tag{1}$$

The results demonstrated that all four groups had a statistically significant decrease in bacterial viability compared to the control ($P < 0.05$) (Fig. 3). Bacterial viability of Group 2 and 3 was lower than that in Group 1 ($P < 0.05$). Group 2 exhibited lower bacterial viability than Group 3 ($P < 0.05$). The Group 4 resulted in the lowest bacterial viability compared to the other four groups.

The live and dead *E. faecalis* images exhibited similar trends to those in Fig. 3 (Fig. 4). As expected, almost no dead bacteria were observed in the control group, and Groups 2—4 exhibited even more dead *E. faecalis* than Group 1. Notably, Groups 2 and 4 exhibited a higher number of dead *E. faecalis* than Group 3.

Cell viability test

In this study, cell viability (%) was determined using Equation (2), The calculated cell viability (%) was thereafter compared between the groups.

$$\text{Cell viability (\%)} = (\text{Exp.} - \text{Blank}) / (\text{Control} - \text{Blank}) \times 100 \tag{2}$$

A statistically significant difference was observed between MC3T3 cells cultured in the control group and Group 1 ($P < 0.05$) (Fig. 5). Group 1 exhibited approximately 25% increase in cell proliferation. However, the Groups 2—4 did not result in a statistically significant difference when compared to Group 1 ($P > 0.05$).

The live and dead MC3T3 cells images exhibit a similar trend to those in Fig. 5 (Fig. 6). In particular, compared to the control group, the number of live cells in Groups 1—4 significantly increased. However, live images of Groups 1—4 did not exhibit any significant difference.

Table 2   List of primers used for real-time PCR.

Primer name	Sequence	Reference
OCN _ F	5′-GCAATAAGGTAGTGAACAGACTCC	NM_007541
OCN _ R	5′-GCGTTTGTAGGCGGTCTTCAAG	
ALPL _ F	5′-CCAGCAGGTTTCTCTCTTGG	NM_001271630
ALPL _ R	5′-GGGATGGAGGAGAGAAGGTC	
RUNX2 _ F	5′-GCAGCACTCCATATCTCTACT	NM_007431
RUNX2 _ R	5′-TTCCGTCAGCGTCAACAC	
GAPDH _ F	5′-AAGGTCATCCCAGAGCTGAA	NM_008084.3
GAPDH _ R	5′-AGGAGACAACCTGGTCCTCA	

F; forward. R; reverse. OCN; osteocalcin, ALPL; alkaline phosphatase, RUNX2; runt-related transcription factor 2, GAPDH; glyceraldehyde 3 phosphate dehydrogenase.
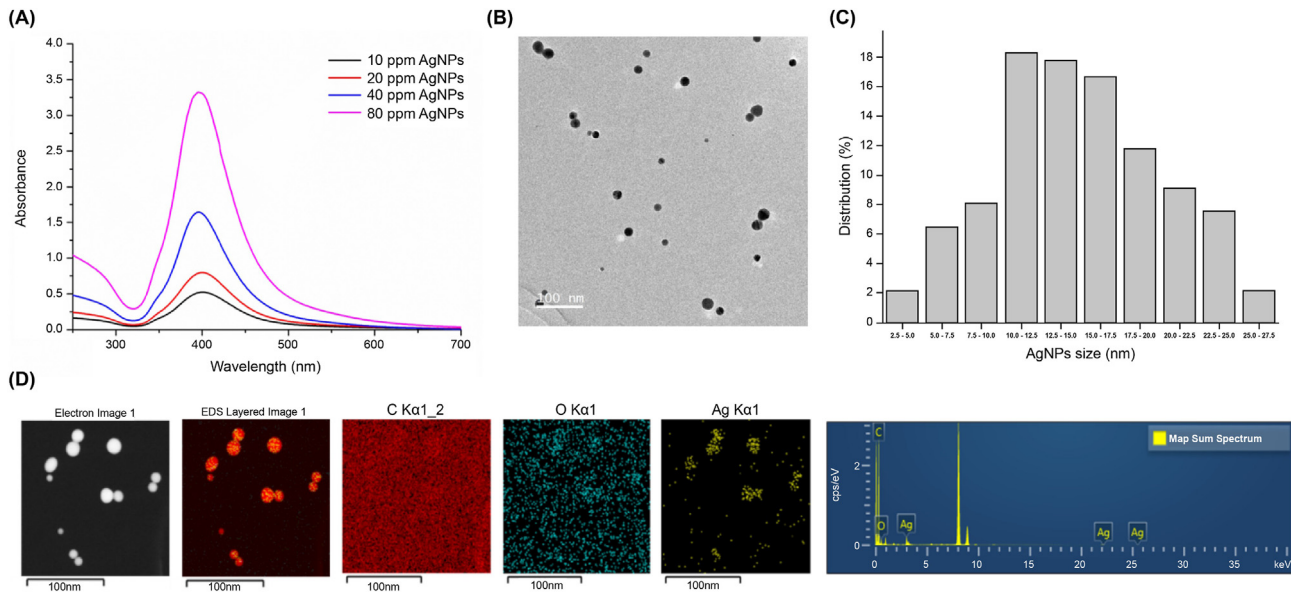
Figure 1 Photo-physicochemical characterization of synthesized silver nanoparticles (AgNPs). (A) Changes in the absorbance graphs according to the concentration of AgNPs, (B) TEM images showing the morphology of AgNPs (scale bar = 100 nm), (C) Analysis of the size distribution of 186 AgNPs, and (D) EDX analysis of AgNPs (scale bar = 100 nm).

Osteogenic potential related gene expression of MC3T3s cells

In comparison to control, Group 1 exhibited a statistically significant increase ($P < 0.05$) in the expression of all three genes, indicating that MTA itself affected osteoblastic potential. Group 2, resulted in increased gene expression compared to that in Group 1, except for OCN ($P < 0.05$). Group 3 significantly increased the expression of all three genes ($P < 0.05$), specifically OCN, ALPL, and RUNX2. Finally Group 4 exhibited a statistically significant increase ($P < 0.05$) in gene expression compared to Groups 2 and 3, except for RUNX2.

Discussion

To confirm the optimal properties of the synthesized AgNPs, UV−Vis spectrophotometry and TEM were used. The AgNPs exhibited a symmetric absorption graph at 400 nm, which is attributed to surface plasmon resonance in Fig. 1(A).[16] Furthermore, as observed in the TEM images, the AgNPs had an average size of 16 nm. The antibacterial efficacy of AgNPs is influenced by their size. In a study comparing sizes ranging from 5 to 100 nm, the highest antibacterial efficacy was observed for sizes approximately 10 nm.[17] Therefore, the AgNPs synthesized in this study may also have sufficient antibacterial efficacy owing to their average size.

In Fig. 2(B), there was no statistically significant difference in R_a among the specimens in Groups 1−4. This suggests that the variation in the surface area due to group differences can be disregarded when the specimen size is the same. While Groups 2 and 4 exhibited lower pH values even after storing the specimens in dH$_2$O for 4 h owing to the presence of acetic acid from the synthesized AgNPs, the difference was negligible, with an average difference of only 0.2, as shown in Fig. 2(C).

The high resistance of *E. faecalis* to RCT is due to its strong attachment to dentinal tubules through collagen-binding proteins.[18−20] However, previous studies have
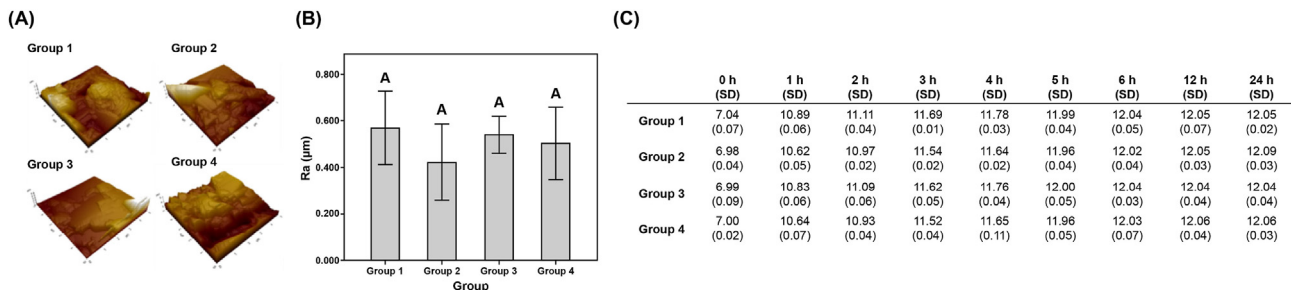

	0 h (SD)	1 h (SD)	2 h (SD)	3 h (SD)	4 h (SD)	5 h (SD)	6 h (SD)	12 h (SD)	24 h (SD)
Group 1	7.04 (0.07)	10.89 (0.06)	11.11 (0.04)	11.69 (0.01)	11.78 (0.03)	11.99 (0.04)	12.04 (0.05)	12.05 (0.07)	12.05 (0.02)
Group 2	6.98 (0.04)	10.62 (0.05)	10.97 (0.02)	11.54 (0.02)	11.64 (0.02)	11.96 (0.04)	12.02 (0.04)	12.05 (0.03)	12.09 (0.03)
Group 3	6.99 (0.09)	10.83 (0.06)	11.09 (0.06)	11.62 (0.05)	11.76 (0.04)	12.00 (0.05)	12.04 (0.03)	12.04 (0.04)	12.04 (0.04)
Group 4	7.00 (0.02)	10.64 (0.07)	10.93 (0.04)	11.52 (0.04)	11.65 (0.11)	11.96 (0.05)	12.03 (0.07)	12.06 (0.04)	12.06 (0.03)

Figrue 2 Surface roughness (R_a) and pH changes of the fabricated four samples. (A) Atomic force microscopy 3D images of the surfaces of the four groups (x axis = 5 μm and y axis = 5 μm), (B) Comparison of R_a, the different capital alphabet represented statistical difference between the groups ($P < 0.05$), and (C) pH changes for 1 d, data are presented as mean values and standard deviation (SD).
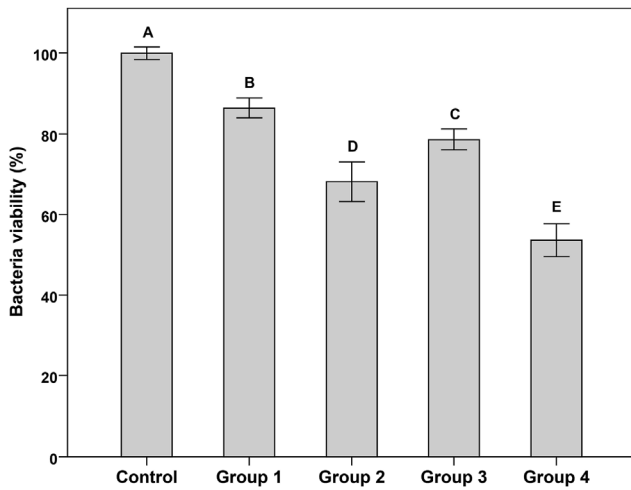
Figure 3 Observation of changes in bacterial viability using 3-(4,5-demethylthiazol-2-yl)-2,5-diphenyltetrazolium bromide (MTT) assay when *E. faecalis* was in direct contact with the samples of each group. Control group referred to the bacterial viability of *E. faecalis* that did not contact MTA. Groups 1—4 represented the percentage of bacterial viability compared to the control, and the capital alphabet indicated a statistical difference between the groups ($P < 0.05$).

Figure 5 Observation of changes in cell viability using **water-soluble tetrazolium (**WST) assay when MC3T3 cells were incubated in each extracted medium. The control group referred to the cell viability of MC3T3 cells incubated in growth medium. Groups 1—4 represented the percentage of cell viability compared to the control, and the different capital alphabets indicated a statistical difference between the groups ($P < 0.05$).

shown that *E. faecalis* has a low survival rate in media with high alkalinity.[21] Groups 2 and 4 exhibited lower pH values even after storing the specimens in dH$_2$O for 4 h owing to the presence of acetic acid from the synthesized AgNPs, the difference was negligible, with an average difference of only 0.2 (Fig. 2(C)).

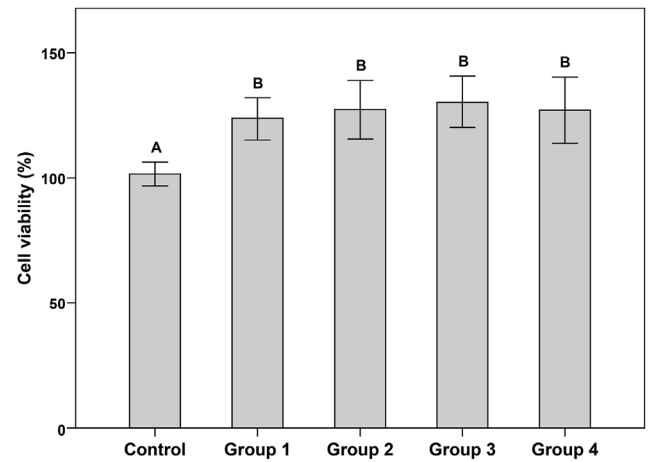Fluoride inhibits glycolytic enzymes, which can undermine bacterial metabolism.[13] Under fluoride exposure conditions, *E. faecalis* exhibits serious modifications in its carbohydrate transport metabolism and growth inhibition.[14] Therefore, in this study, when 1% CaF$_2$ was added to MTA, more fluoride was released to inhibit the metabolism of *E. faecalis*, exhibiting a higher antibacterial efficacy (Figs. 3 and 4). AgNPs have a high surface-area-to-volume ratio and can continuously release Ag ions,[22] which can attach to sulfur proteins of the bacterial membrane owing to electrostatic attraction and induce osmotic pressure to rupture
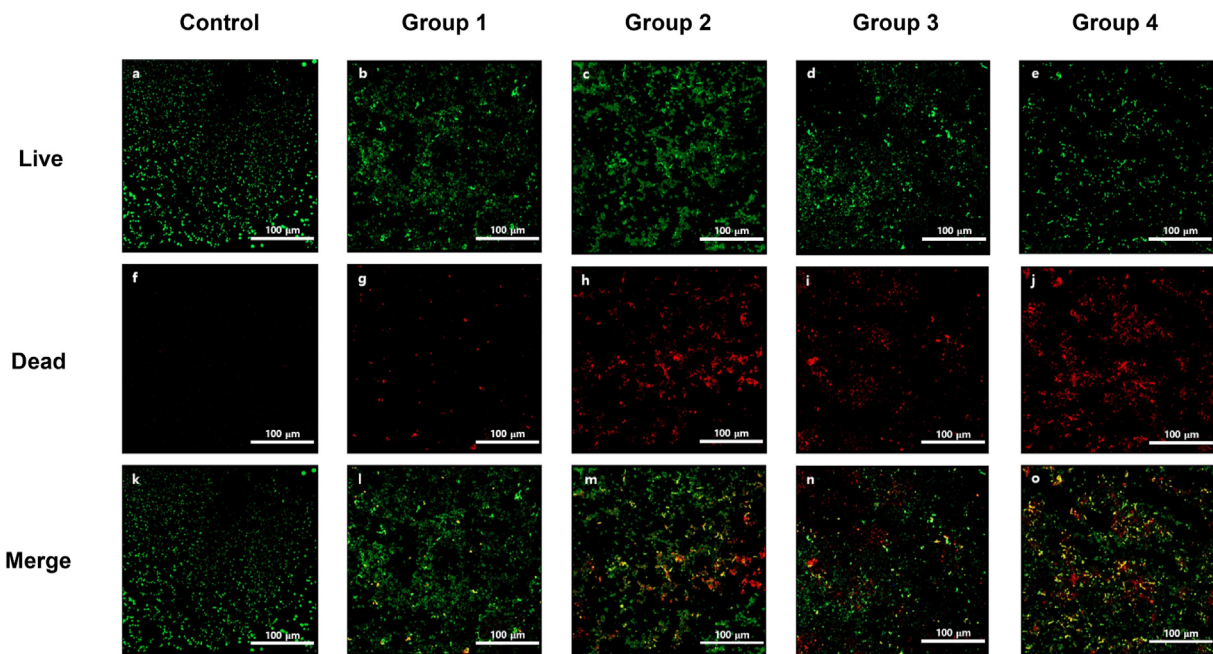

Figure 4 Results of the live/dead images of *E. faecalis* obtained through direct contact with each fabricated specimen. The control group comprised *E. faecalis* without MTA contact. The scale for all images shown was 100 μm.
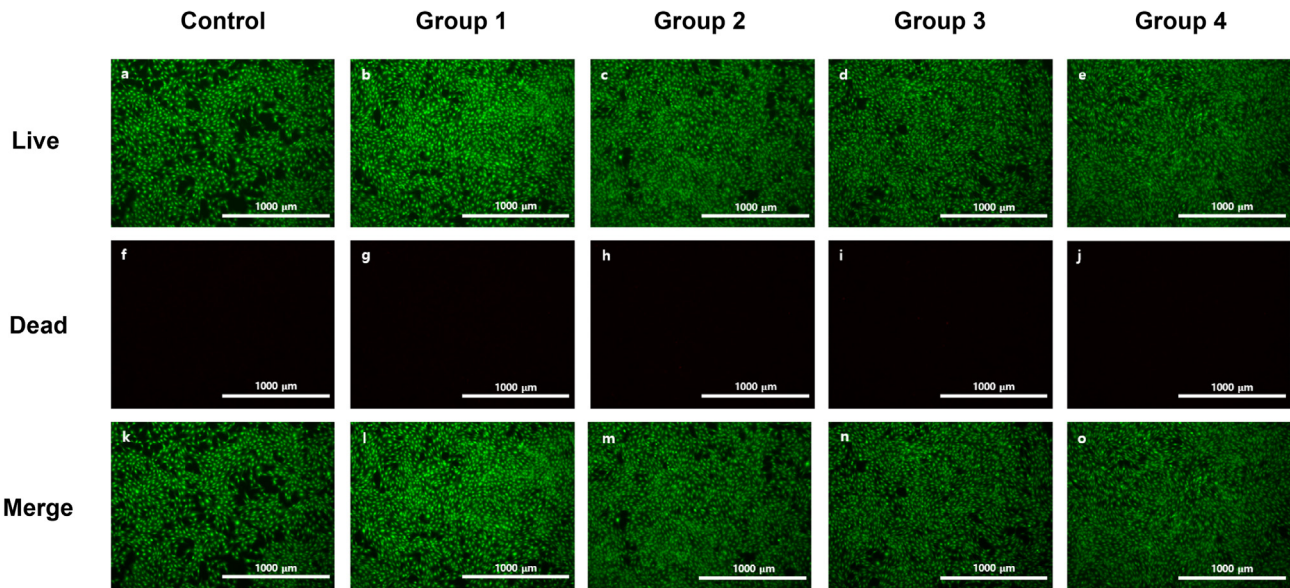
Figure 6 Results of the live/dead cell viability images for MC3T3 cells obtained by incubating in extracted medium. The control group comprised MC3T3 cells incubated in growth medium. The scale for all images shown was 1000 μm.

bacteria.[23–25] In a study to determine the minimum bactericidal concentration (MBC) of AgNPs against *E. faecalis*, AgNPs made using 0.06 M $AgNO_3$ had an MBC of 25–50 ppm against *E. faecalis*.[26] The AgNPs used in this study were made using 0.11 M $AgNO_3$ and were used at a concentration of 50 ppm; thus, they can have sufficient antibacterial efficacy against *E. faecalis*. (Figs. 3 and 4). Furthermore, Group 4 exhibited the highest antibacterial efficacy against *E. faecalis* through different pathways, suggesting that the combination of AgNPs and CaF_2 may have a synergistic effect in inhibiting the growth of *E. faecalis*.

MTA has been shown to promote the proliferation of various cell lines such as human alveolar osteoblasts.[27] In this study, MC3T3 cells, known as pre-osteoblasts, were utilized, which are the most commonly employed cells for evaluating osteogenesis, osteoblast markers, and calcification. Similarly, in this study, MTA increased the viability of MC3T3-E1 cells (Figs. 5 and 6). However, the addition of

AgNPs and fluoride for antimicrobial purposes can potentially cause cytotoxicity. AgNPs have been shown to decrease cell viability in various cell lines and can induce apoptosis through ROS and mitochondrial pathways.[28–30] Additionally, fluoride could affect cell metabolism, with low concentrations having an anabolic effect that could aid in cell proliferation; however, at certain levels, it could inhibit cell proliferation and enzymes such as acid phosphatase.[31–33] In contrast, some studies have suggested that the addition of AgNPs and CaF_2 to MTA does not decrease cell viability.[34,35] Similarly, in this study, the addition of AgNPs and CaF_2 did not decrease cell viability (Figs. 5 and 6). Even Group 4, cell viability did not decrease compared to Group 1. This study complemented the results of the WST test with live/dead cell images for the control group and Groups 1–4.

As mentioned earlier, MTA not only exhibited no cytotoxicity on MC3T3-E1 cells but also increased the mRNA
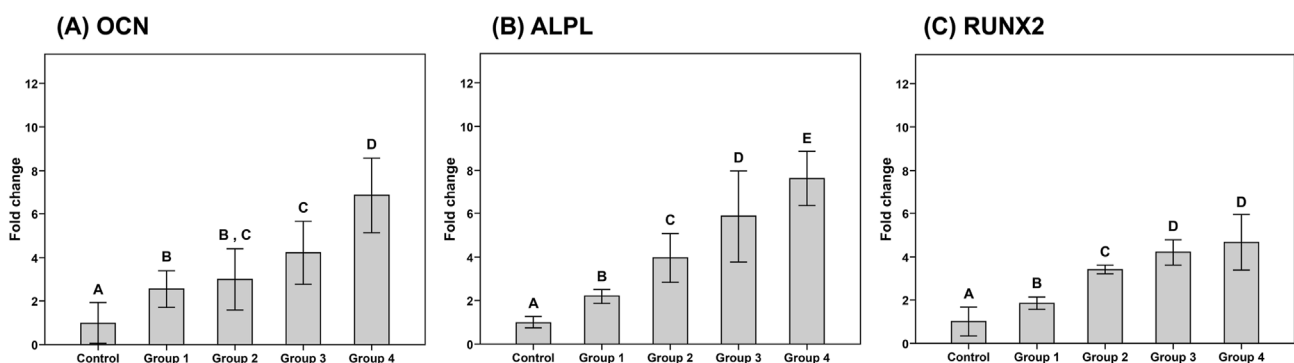

Figure 7 Osteogenic potential gene expression after treatment with each gene such as osteocalcin (OCN), alkaline phosphatase (ALPL), runt-related transcription factor 2 (RUNX2). Different capital alphabets referred to different gene expression levels ($P < 0.05$). The glyceraldehyde 3 phosphate dehydrogenase (GAPDH) gene was used as a housekeeping gene, and the expression level of each gene was represented as fold change compared to the control.

expression of OCN, ALPL, and RUNX2.[10,36] AgNps activated TGF-β/BMP signaling to aid in osteogenic differentiation and increase the gene expression of OCN, RUNX2, and ALPL.[37] In addition, using fluoride at the micromolar level increased OCN and RUNX2 gene expression in MC3T3-E1 cells through RUNX2 signaling.[15] As the results of this study showed, CaF$_2$ was more beneficial than AgNPs for the expression of ALPL and RUNX2 (Fig. 7). When AgNPs and CaF$_2$ were used together, it was expected that Group 4, excluding RUNX2, would exhibit the highest gene expression because each substance triggered a different pathway of osteogenic differentiation.

Despite these results, this study has several limitations. First, cell viability and PCR results were obtained only after 1 d, and future studies will require long-term experimental data. Second, the bacterial viability test was performed with only one bacterial strain, *E. faecalis*, while various bacteria can cause RCT failure, indicating the need to test more bacterial strains. Third, while the antibacterial mechanism of AgNPs and CaF$_2$ has been accurately reported, there is insufficient information on how these two components increase osteogenic gene expression.

Declaration of competing interest

The authors deny any conflicts of interest related to this study.

Acknowledgements

References

1. Mustafa M, Almuhaiza M, Alamri HM, et al. Evaluation of the causes of failure of root canal treatment among patients in the City of Al-Kharj, Saudi Arabia. *Niger J Clin Pract* 2021;24: 621−8.
2. Ashley M, Harris I. The assessment of the endodontically treated tooth. *Dent Update* 2001;28:247−52.
3. Kakehashi S, Stanley H, Fitzgerald R. The effects of surgical exposures of dental pulps in germ-free and conventional laboratory rats. *Oral Surg Oral Med Oral Radiol* 1965;20:340−9.
4. Prada I, Micó-Muñoz P, Giner-Lluesma T, Micó-Martínez P, Collado-Castellano N, Manzano-Saiz A. Influence of microbiology on endodontic failure. Literature review. *Med Oral Patol Oral Cir Bucal* 2019;24:e364.
5. Von Arx T. Apical surgery: a review of current techniques and outcome. *Saudi Dent J* 2011;23:9−15.
6. Chong B, Pitt Ford T, Hudson M. A prospective clinical study of Mineral Trioxide Aggregate and IRM when used as root-end filling materials in endodontic surgery. *Int Endod J* 2003;36: 520−6.
7. Von Arx T. Failed root canals: the case for apicoectomy (periradicular surgery). *JOMS* 2005;63:832−7.
8. Lindeboom JA, Frenken JW, Kroon FH, van den Akker HP. A comparative prospective randomized clinical study of MTA and IRM as root-end filling materials in single-rooted teeth in endodontic surgery. *Oral Surg Oral Med Oral Pathol Oral Radiol Endod* 2005;100:495−500.
9. Kim RJ, Kim MO, Lee KS, Lee DY, Shin JH. An in vitro evaluation of the antibacterial properties of three mineral trioxide aggregate (MTA) against five oral bacteria. *Arch Oral Biol* 2015; 60:497−502.
10. Maeda T, Suzuki A, Yuzawa S, Baba Y, Kimura Y, Kato Y. Mineral trioxide aggregate induces osteoblastogenesis via Atf6. *Bone-KEy Rep* 2015;2:36−43.
11. Bruna T, Maldonado-Bravo F, Jara P, Caro N. Silver nanoparticles and their antibacterial applications. *Int J Mol Sci* 2021;22:7202.
12. Halkai KR, Mudda JA, Shivanna V, Rathod V, Halkai R. Antibacterial efficacy of biosynthesized silver nanoparticles against *Enterococcus faecalis* biofilm: an in vitro study. *Contemp Clin Dent* 2018;9:237−41.
13. Marquis RE. Antimicrobial actions of fluoride for oral bacteria. *Can J Microbiol* 1995;41:955−64.
14. Li G, Shi M, Zhao S, et al. RNA-Seq comparative analysis reveals the response of Enterococcus faecalis TV4 under fluoride exposure. *Gene* 2020;726:144197.
15. Lee M, Arikawa K, Nagahama F. Micromolar levels of sodium fluoride promote osteoblast differentiation through Runx2 signaling. *Biol Trace Elem Res* 2017;178:283−91.
16. Cinteza LO, Scomoroscenco C, Voicu SN, et al. Chitosan-stabilized Ag nanoparticles with superior biocompatibility and their synergistic antibacterial effect in mixtures with essential oils. *Nanomaterials* 2018;8:826.
17. Agnihotri S, Mukherji S, Mukherji S. Size-controlled silver nanoparticles synthesized over the range 5−100 nm using the same protocol and their antibacterial efficacy. *RSC Adv* 2014;4: 3974−83.
18. Hubble T, Hatton J, Nallapareddy S, Murray B, Gillespie M. Influence of *Enterococcus faecalis* proteases and the collagen-binding protein, Ace, on adhesion to dentin. *Oral Microbiol Immunol* 2003;18:121−6.
19. Stuart CH, Schwartz SA, Beeson TJ, Owatz CB. *Enterococcus faecalis*: its role in root canal treatment failure and current concepts in retreatment. *J Endod* 2006;32:93−8.
20. Sundqvist G, Figdor D, Persson S, Sjögren U. Microbiologic analysis of teeth with failed endodontic treatment and the outcome of conservative re-treatment. *Oral Surg Oral Med Oral Pathol Oral Radiol Endod* 1998;85:86−93.
21. Appelbe OK, Sedgley CM. Effects of prolonged exposure to alkaline pH on *Enterococcus faecalis* survival and specific gene transcripts. *Oral Microbiol Immunol* 2007;22:169−74.
22. Bapat RA, Chaubal TV, Joshi CP, et al. An overview of application of silver nanoparticles for biomaterials in dentistry. *Mater Sci Eng, C* 2018;91:881−98.
23. Khorrami S, Zarrabi A, Khaleghi M, Danaei M, Mozafari M. Selective cytotoxicity of green synthesized silver nanoparticles against the MCF-7 tumor cell line and their enhanced antioxidant and antimicrobial properties. *Int J Nanomed* 2018;13: 8013.
24. Ramkumar VS, Pugazhendhi A, Gopalakrishnan K, et al. Biofabrication and characterization of silver nanoparticles using aqueous extract of seaweed Enteromorpha compressa and its biomedical properties. *Biotechnol Rep* 2017; 14:1−7.
25. Durán N, Nakazato G, Seabra AB. Antimicrobial activity of biogenic silver nanoparticles, and silver chloride nanoparticles: an overview and comments. *Appl Microbiol Biotechnol* 2016;100:6555−70.
26. Akmaz S, Dilaver Adıgüzel E, Yasar M, Erguven O. The effect of Ag content of the chitosan-silver nanoparticle composite material on the structure and antibacterial activity. *Adv Mater Sci Eng* 2013;2013.

27. Karygianni L, Proksch S, Schneider S, et al. The effects of various mixing solutions on the biocompatibility of mineral trioxide aggregate. *Int Endod J* 2016;49:561—73.

28. Han JW, Gurunathan S, Jeong JK, et al. Oxidative stress mediated cytotoxicity of biologically synthesized silver nanoparticles in human lung epithelial adenocarcinoma cell line. *Nanoscale Res Lett* 2014;9:1—14.

29. Gurunathan S, Jeong JK, Han JW, Zhang XF, Park JH, Kim JH. Multidimensional effects of biologically synthesized silver nanoparticles in *Helicobacter pylori, Helicobacter felis*, and human lung (L132) and lung carcinoma A549 cells. *Nanoscale Res Lett* 2015;10:1—17.

30. Carlson C, Hussain SM, Schrand AM, et al. Unique cellular interaction of silver nanoparticles: size-dependent generation of reactive oxygen species. *J Phys Chem B* 2008;112:13608—19.

31. Whitford GM. *The Metabolism and Toxicity of Fluoride*, fifteenth ed. Karger Publishers, 1989:159—64.

32. Agalakova NI, Gusev GP. Molecular mechanisms of cytotoxicity and apoptosis induced by inorganic fluoride. *Int Sch Res Notices* 2012;2012.

33. Wu P, Sun Z, Lv X, Pei X, Manthari RK, Wang J. Fluoride induces autoimmune orchitis involved with enhanced IL-17A secretion in mice testis. *J Agric Food Chem* 2019;67: 13333—43.

34. Zand V, Lotfi M, Aghbali A, et al. Tissue reaction and biocompatibility of implanted mineral trioxide aggregate with silver nanoparticles in a rat model. *Iran Endod J* 2016;11: 13—6.

35. Samiei M, Ghasemi N, Asl-Aminabadi N, Divband B, Golparvar-Dashti Y, Shirazi S. Zeolite-silver-zinc nanoparticles: biocompatibility and their effect on the compressive strength of mineral trioxide aggregate. *J Clin Exp Dent* 2017;9: 356—60.

36. Zhang R, Lee P, Lui VC, et al. Silver nanoparticles promote osteogenesis of mesenchymal stem cells and improve bone fracture healing in osteogenesis mechanism mouse model. *Nanomed* 2015;11:1949—59.

37. Qin H, Zhu C, An Z, et al. Silver nanoparticles promote osteogenic differentiation of human urine-derived stem cells at noncytotoxic concentrations. *Int J Nanomed* 2014;9:2469—78.